How to cite: Angew. Chem. Int. Ed. 2024, e202416899
doi.org/10.1002/anie.202416899

CO_2 Hydrogenation

Highly Dispersed ZnO Sites in a ZnO/ZrO_2 Catalyst Promote Carbon Dioxide-to-Methanol Conversion

Xibo Zhang, Xiang Yu, Rafael G. Mendes, Peter Matvija, Angela E. M. Melcherts, Chunning Sun, Xinwei Ye, Bert M. Weckhuysen, and Matteo Monai**

Abstract: ZnO/ZrO_2 catalysts have shown better activity in the CO_2 hydrogenation to methanol compared with single component counterparts, but the interaction between ZnO and ZrO_2 is still poorly understood. In particular, the effect of the ZrO_2 support phase (tetragonal vs. monoclinic) was not systematically explored. Here, we have synthesized ZnO/ZrO_2 catalysts supported on tetragonal ZrO_2 (ZnO/ZrO_2-t) and monoclinic ZrO_2 (ZnO/ZrO_2-m), which resulted in the formation of different ZnO_x species, consisting of sub-nanometer ZnO moieties and large-sized ZnO particles, respectively. ZnO/ZrO_2-t exhibited a higher methanol selectivity (81 vs. 39 %) and methanol yield (1.25 vs. 0.67 mmol g^{-1} h^{-1}) compared with ZnO/ZrO_2-m. The difference in performance was attributed to the redox state and degree of dispersion of Zn, based on spectroscopy and microscopy results. ZnO/ZrO_2-t had a high density of ZnO_x-ZrO_y sites, which favored the formation of active HCOO* species and enhanced the yield and selectivity of methanol along the formate pathway. Such ZnO clusters were further dispersed on ZrO_2-t during catalysis, while larger ZnO particles on ZnO/ZrO_2-m remained stable throughout the reaction. This study shows that the phase of ZrO_2 supports can be used to control the dispersion of ZnO and the catalyst surface chemistry, and lead to enhanced catalytic performance.

Introduction

Converting carbon dioxide (CO_2) into high-value chemicals and fuels is a strategy to reduce greenhouse gas emissions.[1] Among the various conversion pathways of CO_2, the hydrogenation of CO_2 into methanol (CH_3OH) by using renewable hydrogen (H_2) has gained significant attention. CH_3OH may be directly used as fuel, or transformed into olefins and other valuable chemicals via the well-known methanol-to-hydrocarbons (MTH) process.[2] However, the challenge for the catalytic hydrogenation of CO_2 into CH_3OH is that the yield and selectivity towards CH_3OH are still relatively low, mostly due to the competition with the reverse water-gas shift (rWGS) reaction, producing carbon monoxide (CO).[3] While typical solid catalysts used for the CO_2-to-CH_3OH reaction are Cu/ZnO/Al_2O_3,[4] Pd/ZnO,[5] and In_2O_3 systems,[6] many alternative compositions have been proposed in the open literature, such as ZnO/ZrO_2-supported catalyst materials.[7] Interestingly, both stand-alone ZrO_2 and ZnO are known to be active for the rWGS reaction, but the ZnO/ZrO_2 composite catalysts demonstrated up to 86 % CH_3OH selectivity.[8]

Zirconia (ZrO_2) has three possible crystal phases: monoclinic (ZrO_2-m), tetragonal (ZrO_2-t) and cubic (ZrO_2-c).[9] The metastable ZrO_2-t and ZrO_2-c can be obtained by thermal decomposition, chemical evaporation, sol-gel methods, and hydrothermal techniques.[10] Li et al. synthesized pure ZrO_2-m and ZrO_2-t nanoparticles via a simple solvothermal method, using inorganic zirconium salts (e.g., hydrated zirconyl nitrate) and urea in water and methanol, respectively.[11] Bumajdad et al. suggested that mesoporous zirconia nanoparticles with pure ZrO_2-m, ZrO_2-t and ZrO_2-c

[*] Dr. X. Zhang, X. Yu, A. E. M. Melcherts, Dr. C. Sun, Dr. X. Ye, Prof. B. M. Weckhuysen, Dr. M. Monai
Inorganic Chemistry and Catalysis Group, Institute for Sustainable and Circular Chemistry,
Utrecht University, Universiteitsweg 99, 3584 CG Utrecht, The Netherlands
E-mail: b.m.weckhuysen@uu.nl
m.monai@uu.nl

Dr. X. Zhang
State Key Laboratory of Physical Chemistry of Solid Surfaces & Department of Chemistry, College of Chemistry and Chemical Engineering,
Xiamen University, Xiamen 361005, P. R. China

Dr. R. G. Mendes
Soft Condensed Matter Group, Debye Institute for Nanomaterials Science,
Utrecht University, Heidelberglaan 8, 3584 CS Utrecht, The Netherlands

Dr. P. Matvija
Charles University, Faculty of Mathematics and Physics, Department of Surface and Plasma Science, V Holešovičkách 2, Prague, 18000 Praha 8, Czech Republic

phases can be synthesized by thermally treating chitosan- or polyvinyl alcohol-ZrO_x hybrid films in air.[12]

Despite the potential of ZnO/ZrO_2 composite catalyst materials, the interaction between ZnO and ZrO_2 and the nature of the active sites are still not well understood, in particular as a function of ZrO_2 phase (i.e., monoclinic vs. tetragonal), since mixed phases are often used.[13] Wang et al. proposed the interface of ZnO and ZrO_2 in mixed phase Zr–Zn oxide catalysts as the active site for CO_2 adsorption and the subsequent production of formate species.[14] Similarly, Zhang et al. constructed Zn^{2+}–O–Zr^{4+} active sites in a metal–organic framework (i.e., MOF-808), and suggested that Zn^{2+}–O–Zr^{4+} is the active center of the catalytic hydrogenation of CO_2 into CH_3OH instead of Zn_mO_n clusters.[15] However, information is lacking about the evolution of the catalysts under reaction conditions. Therefore, it is of great significance to design ZnO/ZrO_2 catalysts varying the extent and type of interfacial ZnO_x–ZrO_y sites, and to study the reaction mechanism and active phase by various in situ and operando spectroscopy methods.

In this work, the same amount of ZnO was loaded on the surface of ZrO_2-m and ZrO_2-t by impregnation, with the aim to tune the ZnO dispersion. It was found that ZnO formed particles or clusters of different sizes depending on the ZrO_2 support phase. On a ZrO_2-t support, ZnO formed sub-nanometer size clusters with uniform distribution, while large-sized ZnO particles were found on the surface of a ZrO_2-m support. As expected from the larger extent of ZnO–ZrO_2 interface, ZnO/ZrO_2-t showed much higher CH_3OH selectivity (i.e., 81 %) and CH_3OH yield (i.e., 1.25 mmol g^{-1} h^{-1}) compared with ZnO/ZrO_2-m (i.e., 39 % and 0.67 mmol g^{-1} h^{-1}). Operando and in situ spectroscopy experiments revealed that ZnO clusters are redispersed on ZrO-t during catalysis, and that surface formate species are actively involved in the CO_2-to-CH_3OH reaction over ZnO/ZrO_2 catalysts.

Results and Discussion

Two distinct ZnO/ZrO_2 catalyst materials with the same ZnO content were prepared by impregnation on ZrO_2-t and ZrO_2-m as support oxides, followed by calcination at 400 °C for 2 h (see Supporting Information, SI, for more details). Transmission electron microscopy (TEM) images of the starting ZrO_2 supports show that both materials are comprised of irregular nanoparticles (NPs), of ~10–15 nm for the ZrO_2-t support, and slightly larger 20 nm NPs for monoclinic ZrO_2 (ZrO_2-m) (Figure S1). Energy dispersive X-ray (EDX) spectroscopy measurements showed that the Zn content of ZnO/ZrO_2-t and ZnO/ZrO_2-m was 4.7 ± 0.2 and 4.3 ± 0.2 wt %, respectively (Figure S2). In addition, the Brunauer–Emmett–Teller (BET) surface areas of ZrO_2-m and ZrO_2-t were ~56 and ~127 m^2/g, respectively, with minimal changes observed after ZnO loading (Figure S3). The BET surface areas of ZnO/ZrO_2-m and ZnO/ZrO_2-t were ~60 and ~107 m^2/g, respectively. The average pore diameters of ZrO_2-m and ZrO_2-t were comparable, i.e., ~15.6 and ~14.4 nm, respectively, as calculated based on the Barrett–Joyner–Halenda (BJH) method.

The powder X-ray diffraction (PXRD) patterns of the starting ZrO_2-t and ZrO_2-m supports matched the standard XRD references (PDF#71-1282 and PDF#86-1450), proving that two different phases of ZrO_2 have indeed been successfully obtained (Figure 1a). After the addition of Zn and calcination, the PXRD patterns of ZnO/ZrO_2-m showed a new sharp reflection at ~36.2° compared with the ZrO_2-m support, which belongs to the ZnO (101) plane (PDF# 75-0576) (Figure 1b). On the other hand, no diffraction peaks attributed to ZnO were observed in ZnO/ZrO_2-t. These results indicate that ZnO was uniformly dispersed on the surface of the ZrO_2-t support, while large-sized ZnO particles were formed on the ZrO_2-m support.

High-angle angular dark field-scanning transmission electron microscopy (HAADF-STEM) and energy-dispersive X-ray (EDX) spectroscopy analysis were used to further clarify the nanostructure of ZnO/ZrO_2-t and ZnO/ZrO_2-m (Figure 1c–d). The EDX mapping images of ZnO/ZrO_2-t show that Zn atoms were highly dispersed on the surface of the ZrO_2-t support, as there was no obvious ZnO particle aggregation. In contrast, large (> 10 nm) ZnO particles were formed on the surface of the ZrO_2-m support. Aberration-corrected (AC) HAADF-STEM was used to further analyze the distribution of Zn species in the ZnO/ZrO_2-t sample. The EDX mapping images revealed that Zn was evenly distributed at the interface between the ZrO_2-t support particles, forming very small clusters and/or atomic species (Figure 1e).

In order to further analyze the structure of the catalyst materials, the ZnO/ZrO_2 samples were studied by UV/Vis diffuse reflectance spectroscopy (DRS) and Raman spectroscopy. As shown in Figure 2a, the UV/Vis DRS data of both ZnO/ZrO_2-m and ZnO showed an intense absorption band with an onset at ~390 nm, related to the absorption of ZnO.[16] Notably, the intensity of the absorption band related to ZnO species decreased significantly in ZnO/ZrO_2-t, and it exhibited a blue-shift to ~385 nm. Such blue-shifted absorption spectrum indicates an increase in the band gap of the semiconductor, which is consistent with quantum size effects.[17] This further suggests that ZnO was atomically dispersed on the surface of ZrO_2-t.[18] Furthermore, Raman spectroscopy was used to characterize the phase structure of the ZnO/ZrO_2 catalyst (Figure 2b). Under 785 nm laser excitation, the Raman spectrum of ZrO_2-m showed vibrational bands at ~179, 188, 222, 307, 334, 344, 381, 480, 557, 617, and 632 cm^{-1}, which we assigned to the ZrO_2-m phase.[19] An additional vibrational band was observed at ~439 cm^{-1} in the Raman spectrum of ZnO/ZrO_2-m, corresponding to the presence of ZnO. Besides, only vibrational peaks at ~269, 316, 454, and 646 cm^{-1} relating to tetragonal ZrO_2 were observed for ZnO/ZrO_2-t, and no vibrational peaks belonging to ZnO were observed. Therefore, ZnO/ZrO_2 catalysts with two different Zn distribution were obtained by changing the phase of the ZrO_2 support. It can be concluded that the ZnO/ZrO_2-t catalyst exhibited a higher density of ZnO_x-ZrO_y sites compared to ZnO/ZrO_2-m.

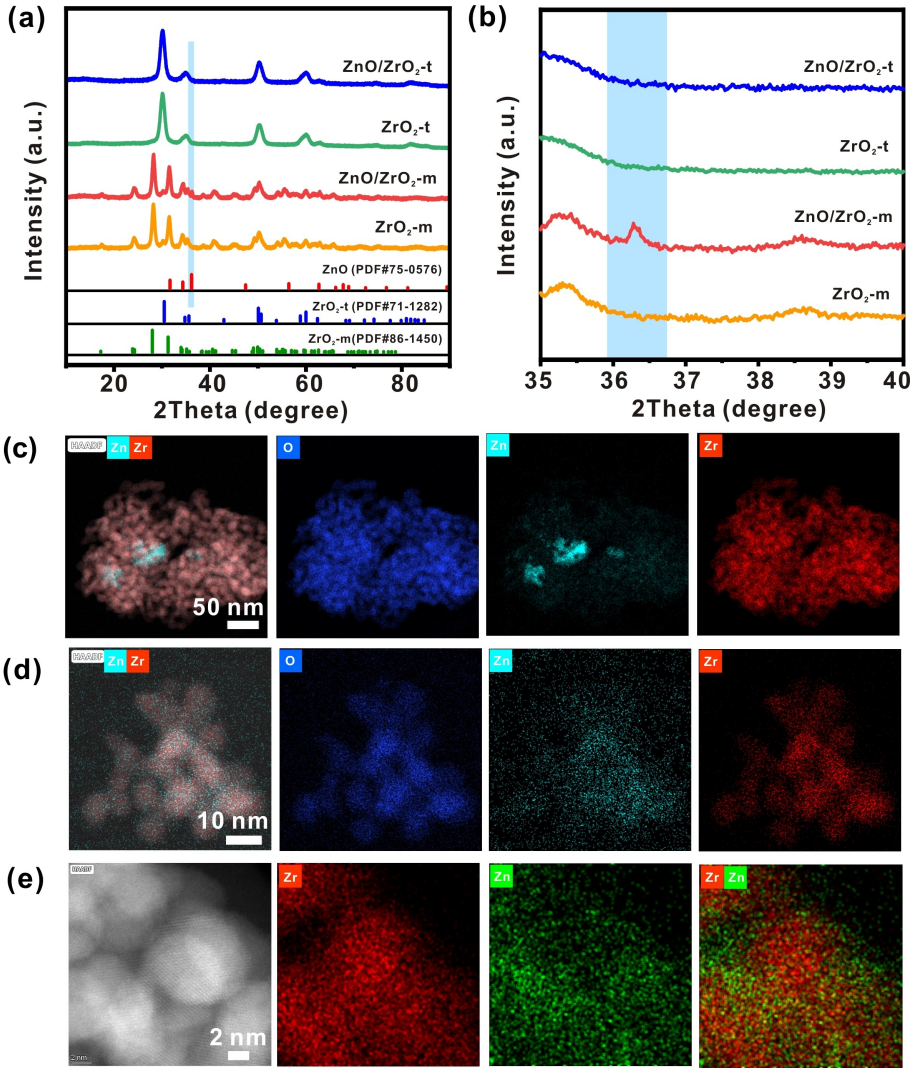

Figure 1. Effect of ZrO_2 phase on ZnO distribution and nanostructure. (a,b) Powder X-ray diffraction (PXRD) patterns of ZrO_2-t, ZrO_2-m, ZnO/ZrO_2-t and ZnO/ZrO_2-m. The blue line corresponds to the reflection of ZnO at ~36.2°. (c,d) High-angle angular dark field-scanning transmission electron microscopy (HAADF-STEM) images, and corresponding energy dispersive X-ray (EDX) spectroscopy mapping images of (c) ZnO/ZrO_2-m and (d) ZnO/ZrO_2-t. (e) Aberration-corrected HAADF-STEM (AC-HAADF-STEM) images of ZnO/ZrO_2-t and corresponding EDX spectroscopy mapping images.

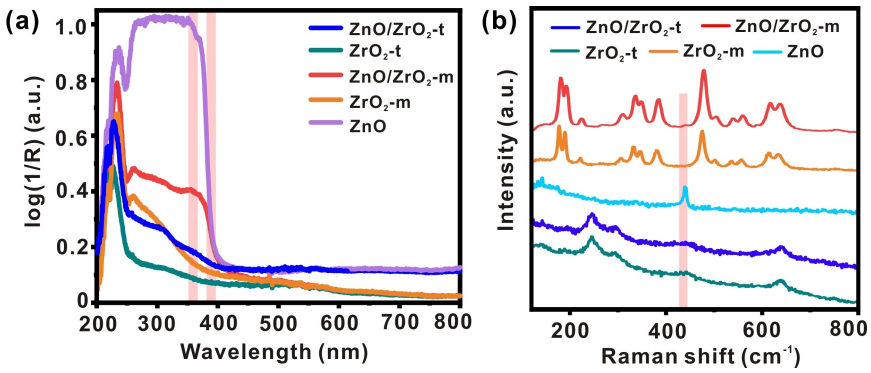

Figure 2. Spectroscopic characterization of the synthesized ZnO/ZrO_2 catalyst materials. UV/Vis DRS data of: (a) ZrO_2-m, ZnO/ZrO_2-m, ZrO_2-t, ZnO and ZnO/ZrO_2-t. The pink lines mark the absorption band of ZnO species in ZnO/ZrO_2-m and ZnO/ZrO_2-t. (b) Raman spectra of: ZnO, ZrO_2-m, ZnO/ZrO_2-m, ZrO_2-t and ZnO/ZrO_2-t. The pink line represents the Raman peak of ZnO.

The difference in extent of ZnO-ZrO_2 interface in the two catalysts is hard to determine quantitatively, but a lower limit may be roughly estimated as follows: If we approximate the sub-nanometer clusters in ZrO_2-t to be at most 1 nm in size, and consider that the ZnO particles in ZrO_2-m are at least 10 nm in size, the ratio of the ZnO-ZrO_2 perimeter in (ZnO/ZrO_2-m)/(ZnO/ZrO_2-t) is at most 1/10.

It is interesting to find that ZnO dispersion could be alerted by changing the ZrO_2 phase (tetragonal or monoclinic). Density functional theory (DFT) calculations were conducted to understand the different dispersion behavior of ZnO between tetragonal and monoclinic ZrO_2. To build a model for the supported ZnO/ZrO_2 catalysts, we used the most stable surfaces of tetragonal ZrO_2 and monoclinic ZrO_2, that is, (101) and (111), respectively (Figure S4).[20] The adsorption energy of a Zn atom on the ZrO_2-t (101) and ZrO_2-m (111) surfaces was calculated. For the adsorption of Zn on ZrO_2-m, only one stable structure was obtained, where Zn replaced a H atom in a hydroxyl group with an adsorption energy of 0.29 eV, indicating unfavorable adsorption of Zn (Figure S5). In contrast, when adsorbing Zn on the ZrO_2-t (101) surface, three different stable structures were obtained. In one of the configurations, Zn replaced a hydrogen atom in a hydroxyl group, while in the other two arrangements, Zn directly coordinated with surface oxygen atoms. The adsorption energies for these structures were −0.64, −0.83, and −0.41 eV, respectively. Therefore, Zn atoms exhibited the strongest adsorption energy (−0.83 eV) when coordinating with surface oxygen atoms on the ZrO_2-t (101) surface, compared to the ZrO_2-m (111) surface, suggesting that a stronger interaction is the reason for enhanced ZnO dispersion on ZrO_2-t (Figure S6–7). The DFT results thus indicate that the surface atomic structure of different phases ZrO_2 affects the adsorption of Zn, consistent with experimental results.

The catalytic performance during CO_2 hydrogenation of the different materials under study was tested in a fixed-bed reactor (see Supporting Information, SI). As shown in Figure 3a, pure ZrO_2-m, ZrO_2-t, and ZnO only produced CO in the CO_2 hydrogenation reaction at 320 °C and 20 bar. The CO yield of ZrO_2-m (0.39 mmol g^{-1} h^{-1}) was significantly higher than that of ZrO_2-t (0.06 mmol g^{-1} h^{-1}) and ZnO (0.03 mmol g^{-1} h^{-1}). On the other hand, both of ZnO/ZrO_2 composite catalysts produced CH_3OH, indicating that the synergistic effects between ZnO and ZrO_2 are beneficial to the formation of CH_3OH. Comparing the catalytic performance of ZnO/ZrO_2-m and ZnO/ZrO_2-t, the CO_2 conversion of ZnO/ZrO_2-t and ZnO/ZrO_2-m were 2.6 % and 2.9 %, respectively. While this conversion value is rather low, it was selected to be in a kinetic regime. It was found that the production rate of CH_3OH in ZnO/ZrO_2-t (i.e., 1.25 mmol g^{-1} h^{-1}) was much higher than that of ZnO/ZrO_2-m (i.e., 0.67 mmol g^{-1} h^{-1}).

Furthermore, ZnO/ZrO_2-t displayed a CH_3OH selectivity of 81 %, which is about twice that of ZnO/ZrO_2-m (i.e., 39 %) (Figure 3a) and was stable for more than 85 h time-on-stream (Figure 3b). The performance of the catalyst materials was comparable or exceeding the one of Zn-based catalysts reported in the literature, even at the relatively low pressure of 20 bar used in this study (Table S1). The difference in BET surface area may partially explain the higher activity of the ZnO/ZrO_2-t catalyst compared to the ZnO/ZrO_2-m catalyst, but do not alone explain the different selectivity observed.

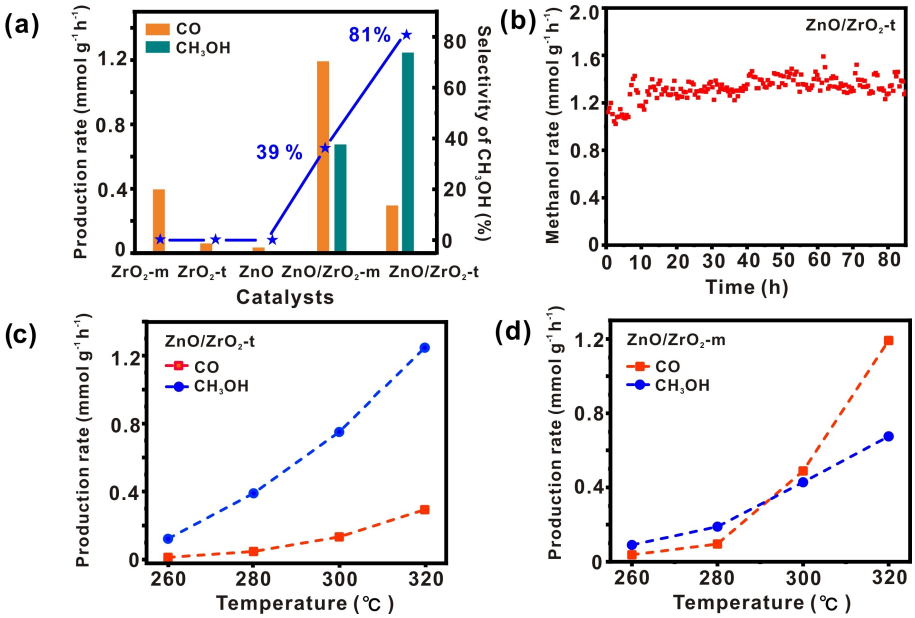

Figure 3. Effect of the ZrO_2 phase on the performance of ZnO/ZrO_2 catalysts in the CO_2-to-CH_3OH reaction. (a) Production rate of CO and CH_3OH and selectivity to CH_3OH for different catalyst materials in CO_2 hydrogenation at 320 °C. (b) Evolution of the production rate of CH_3OH with time on stream over ZnO/ZrO_2-t. (c,d) Production rate of CO and CH_3OH at different reaction temperatures over ZnO/ZrO_2-t and ZnO/ZrO_2-m. (Reaction conditions: 1 g catalyst, reaction pressure = 20 bar, gas composition: CO_2:H_2 = 1/3, and GHSV: 1800 h^{-1}).

The CO_2 hydrogenation catalytic performance of the ZnO/ZrO_2-t and ZnO/ZrO_2-m catalysts was also tested at different reaction temperatures (Figure 3c–d). For the ZnO/ZrO_2-t catalyst, the CH_3OH formation rate was higher than that of CO at all the temperatures tested, while for the ZnO/ZrO_2-m catalyst, the CO production rate increased significantly when the temperature was increased to 300 °C. The CH_3OH yield of ZnO/ZrO_2-t and ZnO/ZrO_2-m began to decrease when the temperature reached 340 °C (Figure S8). This is expected, as the hydrogenation of CO_2 to CH_3OH is an exothermic reaction, and high temperatures are not conducive to the formation of methanol. Due to the competition of rWGS and CH_3OH production reaction, it was not possible to extract sensible values for the apparent activation energies and pre-exponential values by the corresponding Arrhenius plots.[21] Altogether, the higher CH_3OH yield and selectivity of the ZnO/ZrO_2-t catalyst with respect to the ZnO/ZrO_2-m catalyst may be explained by an effect of the different Zn state and/or dispersion (and extent of ZnO-ZrO_2 interface) on the two ZrO_2 supports.

A comparison of the ratio in methanol yield (0.5) and the estimated difference in ZnO-ZrO_2 interface (<0.1) between ZnO/ZrO_2-m and ZnO/ZrO_2-t suggests that the extent of the interface is not the only factor at play in determining the catalytic performance of the catalyst. To further rationalize the observed catalytic trends, we characterized the acid-base properties of the materials under study by NH_3 and CO_2 temperature programmed desorption (TPD) experiments. During NH_3 TPD measurements, a broad peak was observed at ~475–500 °C for ZrO_2-m and ZnO/ZrO_2-m, while a weak band was observed at ~274–287 °C for ZrO_2-t and ZnO/ZrO_2-t, indicating that ZrO_2-m has a relatively stronger acidity (Figure S9a).[22] During CO_2 TPD measurements, the CO_2 desorption peaks of ZrO_2-m and ZnO/ZrO_2-m were observed in the low temperature region (at ~107 and ~88 °C). ZrO_2-t and ZnO/ZrO_2-t exhibited higher temperature CO_2 desorption peaks, indicating that they possess stronger basic sites than ZrO_2-m and ZnO/ZrO_2-m (Figure S9b).[23]

To gain further insights into hydrogen activation behavior of the catalysts, we performed temperature programmed reduction (TPR) experiments with H_2. As expected, we did not observe H_2 consumption in the case of the pure ZrO_2-t and ZrO_2-m supports. Similarly, pure ZnO did not show any H_2 consumption, as the reduction of bulk ZnO is thermodynamically unfavorable even under 1 bar H_2 pressure until temperatures above 1200 °C.[24] On the other hand, ZnO/ZrO_2-t and ZnO/ZrO_2-m showed hydrogen consumption peaks between 300 and 400 °C (Figure S9c). The amount of hydrogen consumed in ZnO/ZrO_2-m and ZnO/ZrO_2-t was ~11.3 and ~1.9 mL/g, respectively. These observations suggest that the ZnO nanostructure and/or the ZrO_2 support phase had an influence on hydrogen activation.

To explain such difference in H_2 uptake between the two catalyst materials, we can propose two hypotheses: (i) ZnO/ZrO_2-t was reduced to a lower degree with respect to ZnO/ZrO_2-m, or (ii) hydrogen spilled over onto ZrO_2-t to a lesser extent than in the case of ZrO_2-m. Theoretically, the amount of hydrogen required for the complete reduction of ZnO in ZnO/ZrO_2-t and ZnO/ZrO_2-m is ~16 and ~15 mL/g, respectively. Therefore, if we were to assume that all H_2 was used for ZnO reduction to metallic Zn, 76 mol.% of Zn would be reduced for ZnO/ZrO_2-m, and 12 mol.% for ZnO/ZrO_2-t. Given that bulk ZnO is not reduced by H_2, and that ZnO is less dispersed (and thus more bulk-like) on ZrO_2-m than in ZrO_2-t, the extent and trend in H_2 uptake are not consistent with ZnO reduction. Therefore, we attribute the observed H_2 consumption to hydrogen spillover from ZnO to ZrO_2. Notably, hydrogen spillover was reported for Cu/ZrO_2-m catalysts,[25] and other reports of hydrogen spillover from metals on ZrO_2 are known.[26]

Since both hydrogen spillover and reduction of ZnO require H_2 activation by dissociative hydrogen adsorption, we studied this step by density functional theory (DFT) calculations. We calculated the adsorption energy of dissociatively adsorbed H_2 on a pure ZnO slab with a (001) termination, and on a Zn atom adsorbed on ZrO_2-t (101) termination (Figure S10–11). The H* adsorption energy at the Zn–O–Zr site in ZnO/ZrO_2-t (101) and the ZnO (001) surface was −0.29 and 0.05 eV, respectively, showing that, thermodynamically, it is easier to form a H* species at a ZnO site in the presence of a ZrO_2 support than on a bulk ZnO surface. This further suggests, based on linear scaling relations and the Hammond postulate, that the activation barrier for H_2 dissociation may be lower on the ZnO_x–ZrO_y sites in ZnO/ZrO_2-t (101) than for pure ZnO. Since a difference in H* adsorption energy will affect the H* coverage at the ZnO sites, we postulate that this, together with the difference in CO_2 adsorption revealed by TPD measurements, could ultimately affect the reaction mechanism and selectivity on the two catalysts.

In order to explore the reaction mechanism of the two differently prepared ZnO/ZrO_2 composite catalysts, the intermediates in the CO_2 hydrogenation reaction were analyzed by operando diffuse reflectance infrared Fourier transform spectroscopy (DRIFTS), and the reaction products were detected by online gas chromatography (GC). Infrared (IR) absorption bands of formate species, CO(g) and methoxy species were observed for the ZnO/ZrO_2-m and ZnO/ZrO_2-t catalysts (Figure 4a–b). Absorption bands at ~1595, 2887, and 1381 cm^{-1} were attributed to the ν_{as}(OCO) stretching vibration, ν(CH) stretching vibration and δ(CH) bending vibration of the adsorbed bidentate HCOO* species.[14] The absorption band at ~2827 cm^{-1} was assigned to the ν(CH_3) stretching vibration of *OCH_3 species.[27] Gaseous CO bands were also observed at ~2174 and ~2113 cm^{-1}. For ZnO/ZrO_2-t, an absorption band was also observed at ~1446 cm^{-1} after 20 min of reaction, and continued to grow in intensity over time (Figure S12). This band was assigned to carbonate (CO_3^{2-}) species.[28] CO_3^{2-} is not a commonly accepted reaction intermediate in the hydrogenation of CO_2 to CH_3OH, and the fact that it slowly accumulates on the surface suggests it is a spectator species. Furthermore, the HCOO* peak (2887 cm^{-1}) of single-component catalytic materials (ZrO_2-t, ZrO_2-m and ZnO) was significantly lower than that of the ZnO/ZrO_2 composite catalysts (Figure S13), suggesting that the formate pathway has an impact on methanol production, and the ZnO-ZrO_2

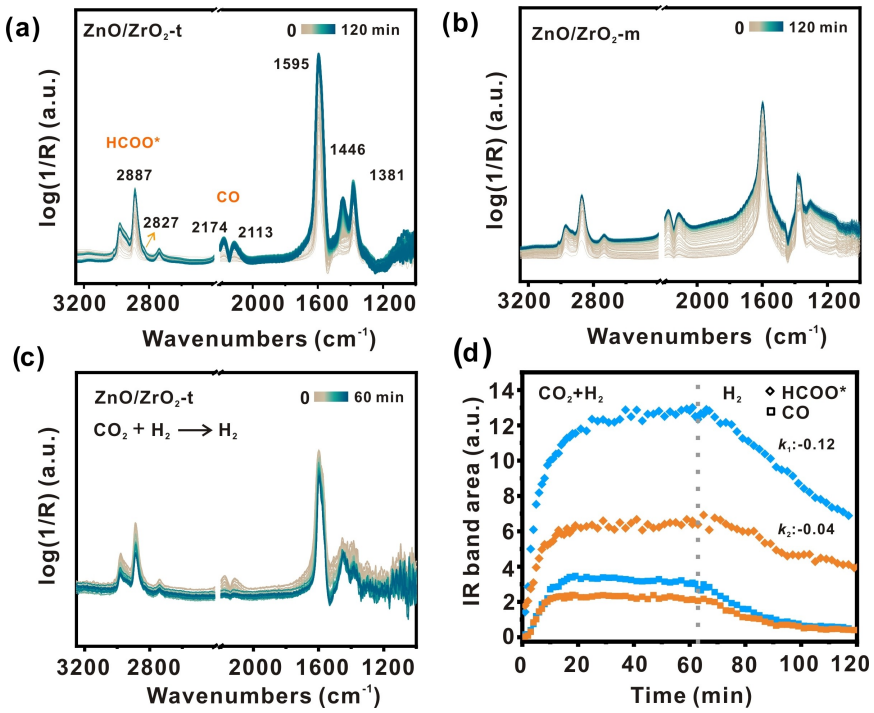

Figure 4. Formation and reactivity of intermediates of the CO_2-to-CH_3OH reaction. Operando DRIFTS data as a function of time during catalytic CO_2 hydrogenation over (a) ZnO/ZrO_2-t and (b) ZnO/ZrO_2-m catalyst materials. (c) DRIFTS spectra as a function of time when switching from CO_2+H_2 to H_2 over ZnO/ZrO_2-t at 320 °C and 10 bar. (d) Area of the HCOO* and CO(g) IR bands when switching from CO_2+H_2 to H_2. (k_1 and k_2 are the slopes of the disappearance of the HCOO* bands for ZnO/ZrO_2-t and ZnO/ZrO_2-m. Blue symbols: ZnO/ZrO_2-t, orange symbols: ZnO/ZrO_2-m). Reaction conditions: $CO_2/H_2=1/3$, reaction temperature = 320 °C, reaction pressure = 10 bar, 1 spectrum min^{-1}).

interface contributes significantly to the formation of HCOO*, thereby enhancing the production of methanol. Compared with the ZnO/ZrO_2-m catalyst, the intensity of the HCOO* absorption bands on ZnO/ZrO_2-t were significantly stronger, indicating that ZnO/ZrO_2-t with a higher density of ZnO_x-ZrO_y sites lead to accumulation of HCOO* species (Figure 4b).

The spectral intensity of HCOO* and gaseous CO bands as a function of time was shown in Figure 4d. For ZnO/ZrO_2-m, the HCOO* band intensity reached a plateau at 20 min, but the intensity value was lower than that of ZnO/ZrO_2-t. On the other hand, ZnO/ZrO_2-m and ZnO/ZrO_2-t showed no obvious difference in the rate and trend of gaseous CO production. The observed CO selectivity is therefore not comparable to the trends observed during catalytic testing (Figure 3), which we attribute to the different operating pressure (10 bar vs. 20 bar).

To gain information about reactive intermediates, we have performed operando DRIFTS experiments, while switching to H_2 after steady state was reached under the CO_2/H_2 reaction mixture (Figure 4c and S14). The areas of the absorption bands of CO(g) (~2174 cm^{-1}), HCOO* (~2887 cm^{-1}) and CO_3^{2-} (~1446 cm^{-1}) in the spectra of ZnO/ZrO_2-t were further analyzed as a function of the time after switching to H_2 (Figure 4d and S15). The intensity of the CO(g) band decreased after switching from CO_2/H_2 to H_2 for both ZnO/ZrO_2-m and ZnO/ZrO_2-t, with similar trends. In addition, the HCOO* band area showed a slight increase and then a decrease for both catalysts. This indicates that H_2 first generated HCOO* by reaction with CO_2, and then further converted the generated HCOO* into methanol. Compared with ZnO/ZrO_2-m, ZnO/ZrO_2-t showed a higher HCOO* band intensity and the rate of decrease in band intensity (slope k_1: −0.12) was significantly higher than that of ZnO/ZrO_2-m (slope k_2: −0.04) (Figure 4d). In addition, the area of the absorption band of CO_3^{2-} (~1446 cm^{-1}) in the spectra of ZnO/ZrO_2-t gradually increased after switching to H_2, indicating that CO_3^{2-} was most probably not an intermediate species of methanol production (Figure S15). When the feed gas CO_2 and H_2 were switched to Ar at 320 °C, the IR band area of HCOO* (~2887 cm^{-1}) in both catalysts did not decrease within 30 min (Figure S16). In addition, the gaseous CO at ~2174 cm^{-1} was quickly purged away within a few minutes. The results are significantly different from the trends observed in Figure 4d and prove that the change in band area is due to reactivity and not desorption.

To study the surface chemistry of the catalyst materials, we performed in situ Near-ambient pressure X-ray photoelectron spectroscopy (NAP-XPS) experiments under CO_2 and H_2. In the C 1s region of the spectrum of ZnO/ZrO_2-t, no signal was observed under ultrahigh vacuum (UHV), but a strong C 1s signal was detected under CO_2+H_2 (Figure 5). The peak of C 1s in ZnO/ZrO_2-t was fitted as $HCOO^-$ (288.4 eV), C–O (286.2 eV), C–C (284.6 eV) and C–H (283.3 eV).[29] The signal intensity of $HCOO^-$ increased with

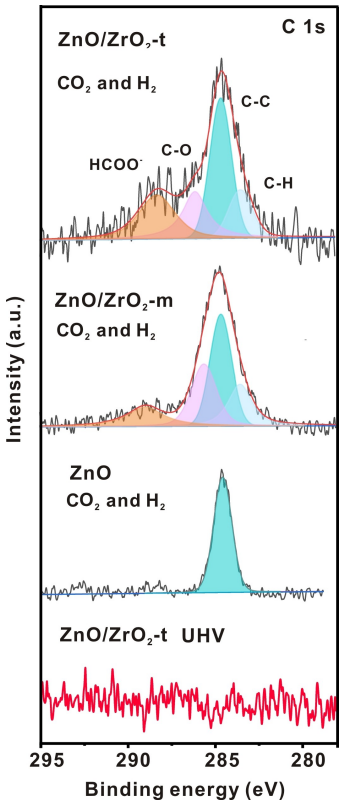

Figure 5. Surface chemistry of ZnO/ZrO_2 materials under CO_2/H_2 gas conditions. In situ NAP-XPS data in the C 1s region for ZnO/ZrO_2-t, ZnO/ZrO_2-m and ZnO at 320 °C in 0.25 mbar CO_2 and 0.75 mbar H_2 and ZnO/ZrO_2-t under ultrahigh vacuum (UHV) conditions.

the increase of the reaction temperature (Figure S17). The results suggest that higher temperature favors the production of $HCOO^-$. When the gas was switched from CO_2 and H_2 to H_2, the $HCOO^-$ signal was reduced, indicating that $HCOO^-$ species were reactive under these conditions (Figure S18). The $HCOO^-$ species were also observed in the C 1s NAP-XPS spectrum of ZnO/ZrO_2-m, but the intensity was much lower than that of ZnO/ZrO_2-t, and only C–C signals were observed in the spectrum of ZnO (Figure 5). The spectra of the Zn Auger LMM spectra revealed that all catalysts exposed Zn^{2+} oxidation state species on the surface under the CO_2/H_2 atmosphere (Figure S19). In summary, the results of the NAP-XPS measurements, albeit being performed at much lower pressures, are consistent with those of the operando DRIFTS measurements, indicating that reactive formate species are preferentially formed at the ZnO/ZrO_2-t interface.

The slow and delayed accumulation of surface CO_3^{2-} species on the ZnO/ZrO_2-t catalyst observed by operando DRIFTS (Figure S15) suggested that the catalyst was changing under CO_2 hydrogenation reaction conditions. To observe possible electronic structure changes of the two ZnO/ZrO_2 catalyst materials during reaction, we performed operando UV/Vis DRS measurements.[30] The procedure of the experiments is shown in Figure S20a. First, the reaction temperature was successively increased to 260, 280, and 300 °C under the reaction atmosphere (i.e., CO_2 and H_2) with 2 h isotherms. Subsequently, the temperature was raised to 320 °C for 6 h, and a gas switching experiment between CO_2 and H_2 was performed after 3 h of reaction. Then, the temperature was gradually decreased to 300, 280 and 260 °C. For the ZnO/ZrO_2-m catalyst, an absorption band belonging to ZnO was clearly visible at ~400 nm and only shifted slightly with temperature during reaction (Figure 6b,d). The intensity of the band edge absorption for ZnO at ~390–410 nm gradually increased as the reaction temperature increased, suggesting the band gap of ZnO became smaller at higher temperature, possibly due to thermal expansion (Figure S20b).[31] The process was indeed reversible, as the absorption band intensity decreased during cooling. Only minor changes in the absorption were observed during gas switching experiments for both ZnO/ZrO_2 catalyst materials, indicating that ZnO was not reduced under the conditions used in this work (Figure S20c).

Notably, the UV/Vis DRS data of ZnO/ZrO_2-t under CO_2 and H_2 at 260 °C were different from that of the fresh catalyst: the intensity of the absorption band at ~250 nm increased sharply, while the absorption bands at ~300 and 358 nm increased slightly in intensity (Figure S21). Moreover, the intensity of the absorption band at ~358 nm decreased upon increasing the temperature to 320 °C, indicating that the ZnO/ZrO_2-t catalyst underwent structural or chemical changes during reaction at higher temperature (Figure 6a,c), which were not reversible during the subsequent cooling process (Figure S20b).

The decrease of intensity of the ligand to metal charge transfer (LMCT) band suggests that the ZnO was either partially reduced, and/or that the already well-dispersed ZnO clusters were further dispersed to form more ZnO_x-ZrO_y sites when the reaction temperature is 320 °C. Based on H_2 TPR results and on thermodynamics of ZnO reduction,[24] it is unlikely that the changes observed by operando UV/Vis DRS are due to ZnO reduction. Moreover, Zn^{2+} reduction was not observed by NAP-XPS under H_2 or CO_2/H_2 atmospheres (Figure S18). On the other hand, the AC-HAADF-STEM image of the used ZnO/ZrO_2-t catalyst showed that Zn was indeed more uniformly dispersed on the ZrO_2-t surface than in the fresh catalyst material (Figure 6f).

The yield of methanol observed by on-line GC measurements during the operando UV/Vis DRS experiments directly illustrates the effect of the dynamic changes of the catalyst on its activity (Figure 6c). The ZnO/ZrO_2-m catalyst showed no significant difference in methanol production during cooling and heating for a certain temperature (Figure S22). In contrast, for the ZnO/ZrO_2-t catalyst, the rate of methanol formation during cooling was higher than that during heating, suggesting that the ZnO structure positively affected the catalytic performance.

We thus show that the higher methanol yield observed is related to an increased density of ZnO_x–ZrO_y sites in the ZnO/ZrO_2-t catalyst due to their restructuring during catalysis. Nonetheless, if we assume that the catalytically active sites for methanol formation are exclusively at the

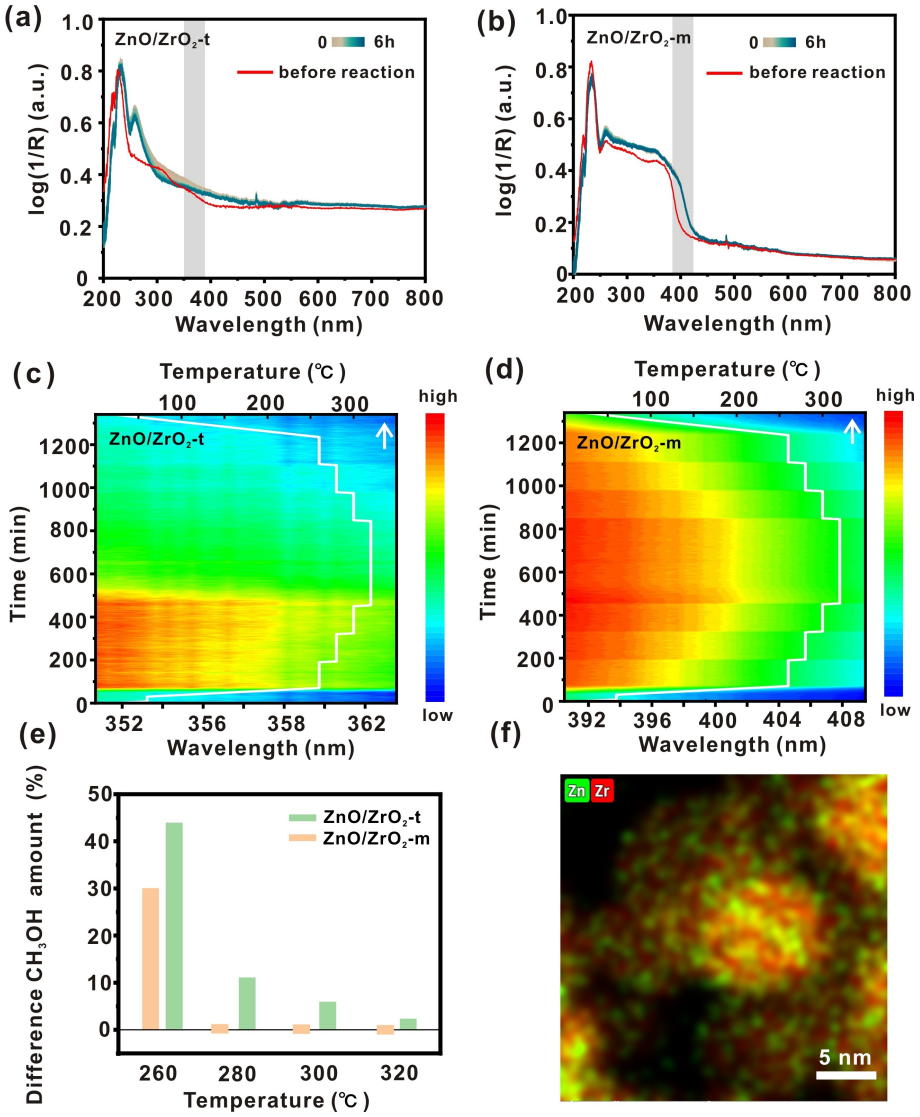

Figure 6. Evolution of ZnO species under CO_2 hydrogenation conditions. Operando UV/Vis DRS data obtained for (a) ZnO/ZrO_2-t and (b) ZnO/ZrO_2-m under CO_2 hydrogenation reaction conditions at 320 °C (grey box marks the absorption band due to ZnO species); (c,d) Contour plots showing the intensities of the UV/Vis absorption during the DRS experiments, for (c) ZnO/ZrO_2-t in the 350–368 nm spectral region and (d)) ZnO/ZrO_2-m in the 390–410 nm region; (e) Difference methanol amount for ZnO/ZrO_2-t and ZnO/ZrO_2-m between the heating and cooling stages. (f) AC-HAADF-STEM image of a used ZnO/ZrO_2-t catalyst material. (Reaction conditions: 1 bar, temperature = 260–320 °C; and gas composition: $CO_2/H_2 = 1/3$).

ZnO-ZrO_2 interface, the intrinsic activity of the interfacial sites in ZnO/ZrO_2-t would be lower than ZnO/ZrO_2-m by at least a factor of 5. Alternatively, it is possible that the extent of the active interface is different in the two catalyst materials, due to a different degree of hydrogen spillover, as suggested by the H_2 TPR results. Moreover, even though bulk ZnO was not active for methanol production, the surface of supported ZnO nanoparticles could also provide active sites for the reaction, as shown by a change in hydrogen stabilization in our DFT calculations. Therefore, future research in controlling the ZnO nanoparticle size and intraparticle distance on both ZrO_2 polymorphs could yield improved methanol synthesis catalysts.

Conclusions

By loading an equal amount of ZnO on the surface of tetragonal ZrO_2 (ZrO_2-t) and monoclinic ZrO_2 (ZrO_2-m), it was found that the nanostructure and surface chemistry of ZnO is affected by the different phases of ZrO_2. Large-sized ZnO particles were observed on the ZrO_2-m surface, while the ZrO_2-t surface contained highly dispersed ZnO clusters. Theoretical calculations indicate that the differences in the adsorption energy of Zn on tetragonal and monoclinic ZrO_2 surfaces lead to distinct dispersion behaviors. The ZnO/ZrO_2-t material showed a higher methanol yield (i.e., 1.25 mmol g^{-1} h^{-1}) and up to 80 % methanol selectivity in the catalytic CO_2 hydrogenation at 20 bar, thereby outperform-

ing the ZnO/ZrO_2-m material. Through operando DRIFTS and in situ NAP-XPS, it was found that HCOO* were active species on both catalyst materials, suggesting that the high density of ZnO_x–ZrO_y sites in ZnO/ZrO_2-t was beneficial to the formation and conversion of HCOO*. However, the different extent of the ZnO–ZrO_2 interface alone did not explain the change in catalytic performance of the two catalysts. H_2 temperature programmed reduction and CO_2 temperature programmed desorption suggest that the type of interface is also important, and can influence the extent of hydrogen spillover and the acid/base properties of the catalyst, in turn affecting the reaction mechanism. Operando UV/Vis diffuse reflectance spectroscopy and transmission electron microscopy indicated that the highly dispersed sub-nanometer ZnO on the surface of ZrO_2-t restructured to form more ZnO_x–ZrO_y interfacial sites to facilitate the production of methanol, while the large-sized ZnO remained stable during reaction. Our findings further reveal the important role of metal oxide interfaces, where both active phase and support functionalities can take part in the reaction mechanism. Future studies should focus on further tuning the interactions between ZnO and ZrO_2, aiming to control the ZnO dispersion on both polymorphs by more advanced synthesis methods and/or related pretreatments.

Acknowledgements

M. Monai and B.M. Weckhuysen acknowledge the Advanced Research Center Chemical Building Blocks Consortium (ARC CBBC) for funding. For access to the electron microscopy methods, we acknowledge the Electron Microscopy Centre of Utrecht University, part of the National Roadmap Infrastructure NEMI, financed under project number 184.034.014 by the Dutch Research Council (NWO). The authors acknowledge the CERIC-ERIC consortium for access to experimental facilities and financial support (proposal number 20227190). P. Matvija is grateful for financial support provided by the Czech Ministry of Education, Youth and Sports (project LM2023072). X. Zhang acknowledge the China Scholarship Council (CSC) for financial support. This work also made use of the Dutch National e-Infrastructure with the support of the SURF Cooperative using grant no. EINF-6932.

Conflict of Interest

The authors declare no conflict of interest.

Data Availability Statement

The data that support the findings of this study are openly available in Data package from [Highly Dispersed ZnO Sites in a ZnO/ZrO2 Catalyst Promote the CO2-to-Methanol Reaction] at https://public.yoda.uu.nl/science/UU01/QJ9IIS.html.

Keywords: CO_2 hydrogenation · Methanol · Zirconia · Zinc oxide · Support effects

[1] a) Y. Liu, D. Deng, X. Bao, *Chem* **2020**, *6*, 2497–2514; b) X. Jiang, X. Nie, X. Guo, C. Song, J. G. Chen, *Chem. Rev.* **2020**, *120*, 7984–8034; c) J. Jia, C. Qian, Y. Dong, Y. F. Li, H. Wang, M. Ghoussoub, K. T. Butler, A. Walsh, G. A. Ozin, *Chem. Soc. Rev.* **2017**, *46*, 4631–4644.
[2] H. Zhan, F. Li, P. Gao, N. Zhao, F. Xiao, W. Wei, L. Zhong, Y. Sun, *J. Power Sources* **2014**, *251*, 113–121.
[3] J. Zhu, F. Cannizzaro, L. Liu, H. Zhang, N. Kosinov, I. A. W. Filot, J. Rabeah, A. Bruckner, E. J. M. Hensen, *ACS Catal.* **2021**, *11*, 11371–11384.
[4] S. Kattel, P. J. Ramirez, J. G. Chen, J. A. Rodriguez, P. Liu, *Science* **2017**, *355*, 1296–1299.
[5] H. Bahruji, M. Bowker, G. Hutchings, N. Dimitratos, P. Wells, E. Gibson, W. Jones, C. Brookes, D. Morgan, G. Lalev, *J. Catal.* **2016**, *343*, 133–146.
[6] A. Tsoukalou, P. M. Abdala, D. Stoian, X. Huang, M. G. Willinger, A. Fedorov, C. R. Muller, *J. Am. Chem. Soc.* **2019**, *141*, 13497–13505.
[7] a) I. Ro, Y. Liu, M. R. Ball, D. H. K. Jackson, J. P. Chada, C. Sener, T. F. Kuech, R. J. Madon, G. W. Huber, J. A. Dumesic, *ACS Catal.* **2016**, *6*, 7040–7050; b) K. Samson, M. Śliwa, R. P. Socha, K. Góra-Marek, D. Mucha, D. Rutkowska-Zbik, J. F. Paul, M. Ruggiero-Mikołajczyk, R. Grabowski, J. Słoczyński, *ACS Catal.* **2014**, *4*, 3730–3741; c) H. Song, D. Laudenschleger, J. J. Carey, H. Ruland, M. Nolan, M. Muhler, *ACS Catal.* **2017**, *7*, 7610–7622.
[8] J. Wang, G. Li, Z. Li, C. Tang, Z. Feng, H. An, H. Liu, T. Liu, C. Li, *Sci. Adv.* **2017**, *3*, e1701290.
[9] Y. Han, J. Zhu, *Top. Catal.* **2013**, *56*, 15–17.
[10] H. Bojari, A. Malekzadeh, M. Ghiasi, *J. Cluster Sci.* **2013**, *25*, 387–395.
[11] W. Li, H. Huang, H. Li, W. Zhang, H. Liu, *Langmuir* **2008**, *24*, 8358–8366.
[12] A. Bumajdad, A. Abdel Nazeer, F. Al Sagheer, S. Nahar, M. I. Zaki, *Sci. Rep.* **2018**, *8*, 3695.
[13] C. Zhang, L. Wang, Y. Chen, X. He, Y. Song, O. M. Gazit, Z. Zhong, *Chem. Eng. J.* **2023**, *475*,146102.
[14] Y. Wang, S. Kattel, W. Gao, K. Li, P. Liu, J. G. Chen, H. Wang, *Nat. Commun.* **2019**, *10*, 1166.
[15] J. Zhang, B. An, Z. Li, Y. Cao, Y. Dai, W. Wang, L. Zeng, W. Lin, C. Wang, *J. Am. Chem. Soc.* **2021**, *143*, 8829–8837.
[16] M. Haase, H. Weller, A. Henglein, *J. Phys. Chem.* **1988**, *92*, 482–487.
[17] W. Zhang, J. Shi, L. Wang, D. Yan, *Chem. Mater.* **2000**, *12*, 1408–1413.
[18] J. Sowik, M. Miodyńska, B. Bajorowicz, A. Mikolajczyk, W. Lisowski, T. Klimczuk, D. Kaczor, A. Zaleska Medynska, A. Malankowska, *Appl. Surf. Sci.* **2019**, *464*, 651–663.
[19] X. Gao, J.-M. Jehng, I. E. Wachs, *J. Catal.* **2002**, *209*, 43–50.
[20] C. Ricca, A. Ringuedé, M. Cassir, C. Adamo, F. Labat, *J. Comput. Chem.* **2015**, *36*, 9–21.
[21] M. S. Frei, C. Mondelli, R. Garcia-Muelas, K. S. Kley, B. Puertolas, N. Lopez, O. V. Safonova, J. A. Stewart, D. Curulla Ferre, J. Perez-Ramirez, *Nat. Commun.* **2019**, *10*, 3377.
[22] F. Yang, G. Li, P. Gao, X.-N. Lv, X. Sun, Z.-H. Liu, H. Fan, *Energy Technol.* **2013**, *1*, 581–586.
[23] L. Lin, G. Wang, F. Zhao, *ChemistrySelect* **2021**, *6*, 2119–2125.
[24] S. Polsilapa, D. R. Sadedin, P. Wangyao, *High Temp. Mater. Processes* **2011**, *30*, 587–592.
[25] K. D. Jung, A. T. Bell, *J. Catal.* **2000**, *193*(2), 207–223.
[26] a) D. L. Hoang, H. Berndt, H. Lieske, *Catal. Lett.* **1995**, *31*, 165–172; b) H. Ishikawa, J. N. Kondo, K. Domen, *Stud. Surf. Sci. Catal.* **1997**, *112*, 73–80.

[27] C. Wu, L. Lin, J. Liu, J. Zhang, F. Zhang, T. Zhou, N. Rui, S. Yao, Y. Deng, F. Yang, W. Xu, J. Luo, Y. Zhao, B. Yan, X. D. Wen, J. A. Rodriguez, D. Ma, *Nat. Commun.* **2020**, *11*, 5767.
[28] A. A. Shaltout, M. A. Allam, M. A. Moharram, *Spectrochim. Acta Part A* **2011**, *83*, 56–60.
[29] Y. Ren, K. Yuan, X. Zhou, H. Sun, K. Wu, S. L. Bernasek, W. Chen, G. Q. Xu, *Chem. Eur. J.* **2018**, *24*, 16097–16103.
[30] J. Goetze, F. Meirer, I. Yarulina, J. Gascon, F. Kapteijn, J. Ruiz-Martinez, B. M. Weckhuysen, *ACS Catal.* **2017**, *7*, 4033–4046.
[31] S. Kumar, P. D. Sahare, *Opt. Commun.* **2012**, *285*, 5210–5216.

Manuscript received: September 3, 2024
Accepted manuscript online: October 8, 2024
Version of record online: ■■, ■■

Research Article

CO_2 Hydrogenation

X. Zhang, X. Yu, R. G. Mendes, P. Matvija, A. E. M. Melcherts, C. Sun, X. Ye, B. M. Weckhuysen,* M. Monai* _____ e202416899

Highly Dispersed ZnO Sites in a ZnO/ZrO_2 Catalyst Promote Carbon Dioxide-to-Methanol Conversion

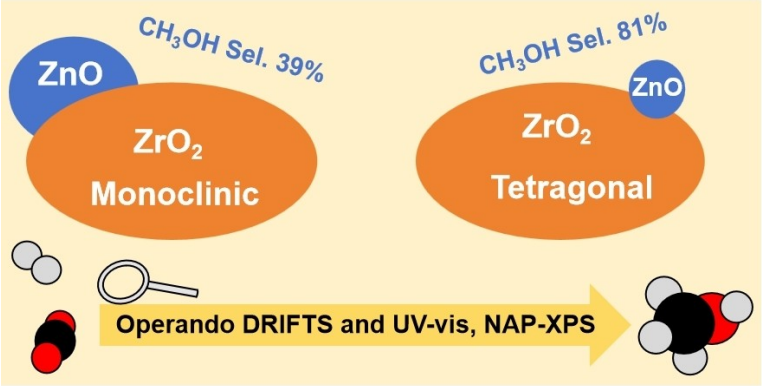

This study examines how ZrO_2 crystal phases influence CO_2 hydrogenation to methanol over ZnO. ZnO on tetragonal zirconia (ZrO_2-t) showed higher activity and selectivity for methanol than on monoclinic zirconia (ZrO_2-m), due to higher ZnO dispersion and an extended ZnO/ZrO_2 interface, which enhances HCOO* intermediate conversion into methanol.